Electronic Supplementary Information for

Three-pole wheel paddle luminescent metal organic framework (LMOF) based on oxygen substituted triazine tricarboxylic acid ligand: recognition and detection of small drug molecules and aromatic amine molecules

*Yao Xiao,[a] Zi Xin You,[a] Yong Heng Xing,[*a] Feng Ying Bai[*a] and Zhan Shi [b]*

a. College of Chemistry and Chemical Engineering, Liaoning Normal University, Dalian City, 116029, P.R. China.

b. State Key Laboratory of Inorganic Synthesis and Preparative Chemistry, College of Chemistry, Jilin University, Changchun 130012, P.R. China

Table of Contents

Materials and Methods.

The ligand H_3TCPT was prepared by literature method and appropriately modified the methods [1]. The specific synthesis steps are as follows: At room temperature, we weighed 6.22 g of p-hydroxybenzoic acid into a 250 mL three-necked flask, then added 20 mL of acetone and 10 mL of water. Meanwhile, we took a beaker and added 10 mL of water to it, then we weighed 3.6 g of sodium hydroxide into the beaker. After the sodium hydroxide was dissolved, we added it to the three-necked flask and kept stirring under the condition of ice-water bath. At this time, the solution was oily.

Then we weighed 2.75 g of cyanuric chloride and it was dissolved in 175 mL of acetone and transfered it to a constant pressure dropping funnel. We added the acetone solution of cyanuric chloride dropwise to the three-necked flask for 1 h. The solution changed from light yellow to white and there was solid precipitation. After the dropwise addition, the three-necked flask was transferred to room temperature for reaction for 2 h. Then the three-necked flask was transferred to an oil bath, and the temperature was raised to 72 °C and refluxed for 6 h. After the reaction was complete, the solution was quickly poured into ice water. The result was 6 g of white solid was obtained by suction filtration under reduced pressure, with a yield of 81.7%. The synthetic route is shown in Scheme 1.

All other original chemical reagents and solvents employed in the present work were purchased from commercial sources and used without further purification. The Bruker AXS TENSOR-27 FT-IR spectrometer was applied to record Infrared spectra in the range of 4000-400 cm^{-1}. UV-vis absorption spectra of solid sample were received from a JASCO V-570 UV/VIS/NIR spectrophotometer with the range of 200-800 nm, and Lambda 35 spectrometer was applied to record the UV-vis absorption spectra of suspension samples in 200-800 nm. Thermogravimetric data was obtained from a PerkinElmer Diamond TG/DTA under nitrogen protection from room temperature to 1100 °C with the heating rate of 10 ℃ •min^{-1}. X-ray powder diffraction (PXRD) patterns were performed on an Advance D8 equipped with Cu-Kα radiation in the range of $5° < 2\theta < 60°$, with a step size of 0.02° (2θ) and a count time of 2 s per step. The HORIBA Fluoromax-4-TCSPC spectrofluorometer which is provided with Pulsed LED sources (200-1000 nm) with 3.2-inch Integrating Sphere was used to measure the fluorescence behavior of the coordination complexes at room temperature. The size and morphology of the material surface was investigated by Scanning Electron Microscope & X-ray Analyzer (SEM, SU8010) and Atomic Force Microscope (AFM, Asylum Research Cypher ES).

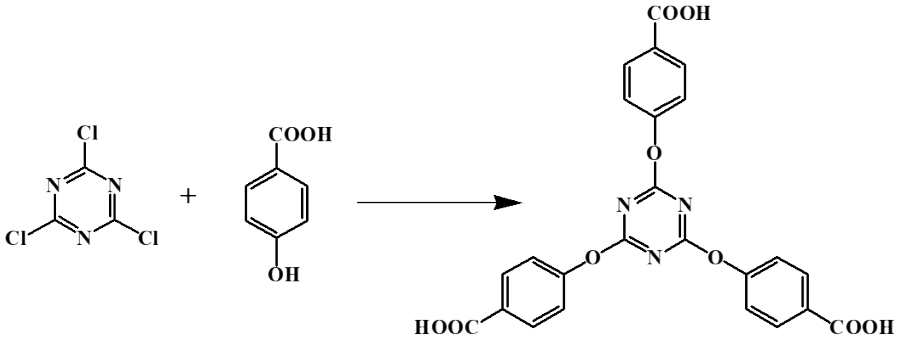

Scheme 1 Synthetic route of 2, 4, 6-tris (p-hydroxyphenoxy) - 1, 3, 5-triazine

Table S1 The crystallographic data of single crystal X-ray diffraction of complexes **1** and **2**[*]

Complexes	**1**	**2**
Formula	$C_{49.5}N_{6.5}O_{22.5}H_{35.5}Cd_3$	$C_{25.5}H_{26.5}N_{3.5}O_{15.5}Zn_2$
M (g mol^{-1})	1418.55	760.95
Crystal system	*Trigonal*	*Hexagonal*
Space group	$P\bar{3}$	*P*63/*m*
a (Å)	17.118(3)	16.8223(18)
b (Å)	17.118(3)	16.8223(18)
c (Å)	13.766(6)	6.8892(14)
α (°)	90	90
β (°)	90	90
γ (°)	120	120
V (Å^3)	3493(2)	1688.4(5)
Z	2	2
D_{calc}	1.349	1.466
Crystal size/mm	0.54×0.33×0.03	0.34×0.22×0.13
F(000)	1404.0	776.0
μ (Mo-Kα)/mm^{-1}	0.973	1.475
θ (°)	1.479～28.408	4.071～25.131
Reflections collected	22290	2538
Independent Reflections (I >2σ(I))	5776	715
Parameters	234	98
$\Delta(\rho)$ (e Å^{-3})	2.60 and -1.17	1.75 and -1.10
Goodness of fit	0.979	0.966
R[a]	0.0965 (0.1385)[b]	0.0740 (0.1275)[b]
wR_2[a]	0.2761 (0.2965)[b]	0.1733 (0.2067)[b]

*[a]$R=\sum \left| F_O-F_C \right| / \sum \left| F_O \right|$, $wR_2=\{\sum[w(F_O^2-F_C^2)^2]/\sum[w(F_O^2)^2]\}^{1/2}$; [$F_O>4\sigma(F_O)$]. [b]Based on all data.

Table S2 Selected bond lengths (Å) and bond angle (°) for complex **1**[*]

Cd(1)-O(1)	2.286(15)	Cd(1)-O(1)$^{\#1}$	2.343(11)
Cd(1)-O(1)$^{\#2}$	1.927(13)	Cd(2)-O(2)	2.181(8)
Cd(2)-O(2)$^{\#1}$	2.181(8)	Cd(2)-O(2)$^{\#2}$	2.181(8)
Cd(3)-O(5)$^{\#3}$	2.373(8)	Cd(3)-O(5)$^{\#4}$	2.373(8)

Cd(3)-O(5)	2.373(8)	Cd(3)-O(4)$^{\#3}$	2.210(8)
Cd(3)-O(4)$^{\#4}$	2.210(8)	Cd(3)-O(4)	2.210(8)
O(1)$^{\#2}$-Cd(1)-O(1)$^{\#1}$	107.0(5)	O(1)-Cd(1)-O(1)$^{\#1}$	96.1(4)
O(1)$^{\#2}$-Cd1-O1	109.3(4)	O(2)-Cd(2)-O(2)$^{\#2}$	107.6(3)
O(2)$^{\#1}$-Cd(2)-O(2)$^{\#2}$	107.6(3)	O(2)-Cd(2)-O(2)$^{\#1}$	107.6(3)
O(5)$^{\#3}$-Cd(3)-O(5)	89.0(3)	O(5)$^{\#3}$-Cd(3)-O(5)$^{\#4}$	89.0(3)
O(5)-Cd(3)-O(5)$^{\#4}$	89.0(3)	O(4)$^{\#4}$-Cd(3)-O(5)$^{\#3}$	129.2(4)
O(4)$^{\#4}$-Cd(3)-O(5)$^{\#4}$	53.7(3)	O(4) -Cd(3)-O(5)$^{\#4}$	129.2(4)
O(4)$^{\#3}$-Cd(3)-O(5) $^{\#3}$	53.7(3)	O(4) -Cd(3)-O(5)$^{\#3}$	119.2(4)
O(4) $^{\#3}$-Cd(3)-O5	129.2(4)	O(4)$^{\#4}$-Cd(3)-O(5)	119.2(4)
O(4)-Cd(3)-O(5)	53.7(3)	O(4) $^{\#3}$-Cd(3)-O(5)$^{\#4}$	119.2(4)
O(4) -Cd(3)-O(4)$^{\#4}$	111.5(2)	O(4)$^{\#3}$-Cd(3)-O(4)	111.5(2)
O(4)$^{\#3}$-Cd(3)-O(4)$^{\#4}$	111.5(2)		

Symmetry transformations used to generate equivalent atoms: #1 +y-x,1-x,+z; #2 1-y,1+x-y,+z; #3 1-y, +x-y, +z; #4 1+y-x, 1-x, +z

Table S3 Selected bond lengths (Å) and bond angle (°) for complex **2***

Zn1-O1	2.09(3)	Zn1-O2	1.953(5)
Zn1-O2$^{\#1}$	1.953(5)	Zn1-O2$^{\#2}$	1.953(5)
O2-Zn1-O2$^{\#2}$	103.058	O2-Zn1-O2$^{\#1}$	103.058
O2$^{\#1}$-Zn1-O2$^{\#2}$	103.058	O2$^{\#2}$-Zn1-O1	120.417
O2$^{\#1}$-Zn1-O1	120.389	O2-Zn1-O1	104.268

Table S4 The IR assignments of ligands and complexes **1** and **2** (cm^{-1})

	H_3L	1	2
ν_{O-H}	3535	3408	3452
ν_{Ar-H}	3008	3086	3060

ν_{ascoo-}	1681	1651	1660
ν_{scoo-}	1373	1361	1356
$\nu_{C=C}/\nu_{C=N}$	1562	1569	1571
ν_{C-N}/ν_{C-C}	1288, 1205	1256, 1210	1254, 1208
ν_{C-O}	1097	1085	1088
δ_{Ar-H}	859, 771	863, 786	876, 772

Table S5 The UV assignments of ligand and complexes **1** and **2**

	Wavelength(nm)	Transition	Types
H_3TCPT	252	π-π*	LLCT
	346	n-π*	LLCT
Complex **1**	247	π-π*	LLCT
	360	n-π*	LLCT
Complex **2**	250	π-π*	LLCT
	355	n-π*	LLCT

Table S6 The detection limits for colchicine, balsalazide disodium and aromatic amine molecules

Analyte	Method	LOD(μM)	Ref
colchicine	fluorometric	24.3	2
		15	3
	This work	4.77 (complex 2)	
		60 (complex 1)	
balsalazide disodium	RP-LC	3.4	4
	This work	0.21 (complex 1)	
		2.7 (complex 2)	
OPD	fluorometric	49.9	5
		30	6
	This work	4.09 (complex 1)	
		16.7 (complex 2)	
MPD	fluorometric	45.7	5
	chemiluminescence	9	
	This work	3.18 (complex 1)	

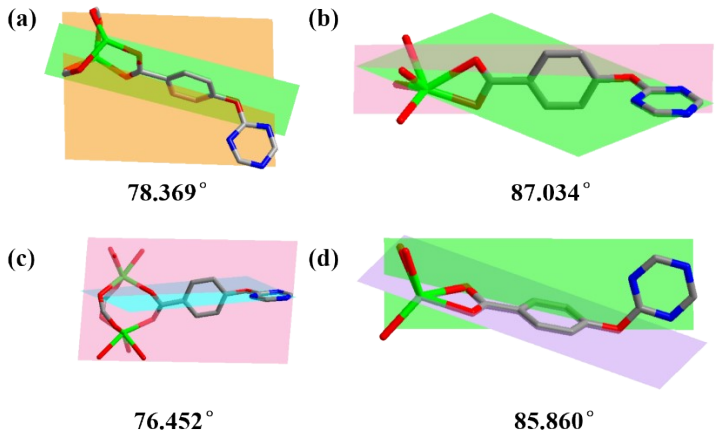

Figure S1 The twist angle between the triazine ring and the benzene ring: (a), (b) for complex 1; (c), (d) for the literature reported

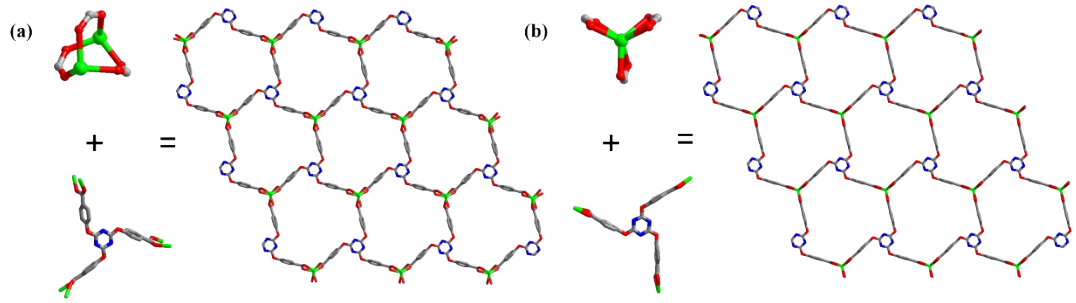

Figure S2 (a) The planar layer structure connected by binuclear building blocks [$Cd_2(COO)_3$] and ligands; (b) The planar layer structure connected by building blocks [$Cd(COO)_3$] and ligands

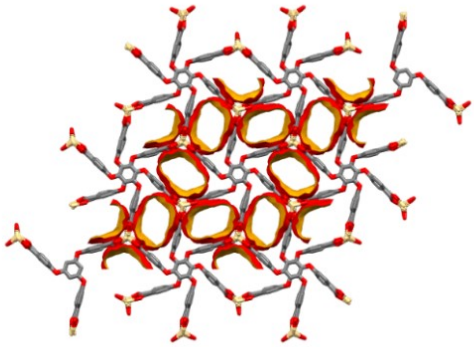

Figure S3 The schematic diagram of the channel of complex **1**

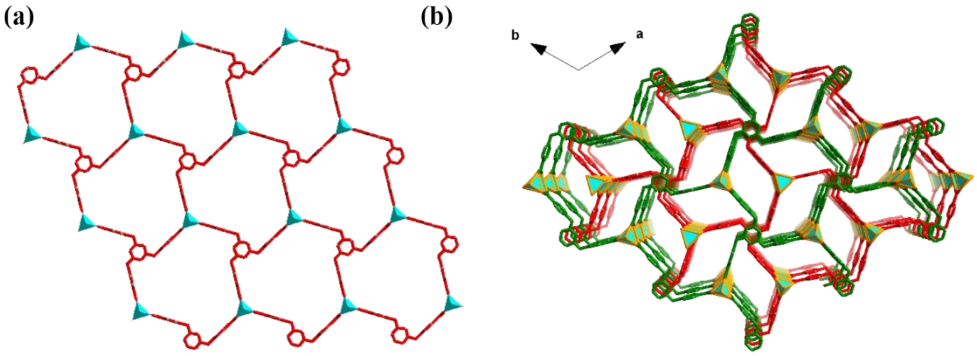

Figure S4 (a) Hexagonal channel; (b) Schematic diagram of three-dimensional interpenetration

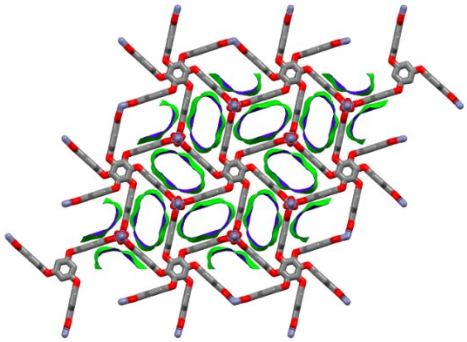

Figure S5 The schematic diagram of the channel of complex **2**

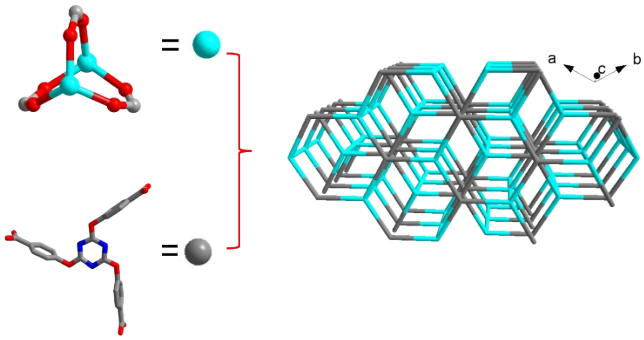

Figure S6 Topological structure of complex **2**

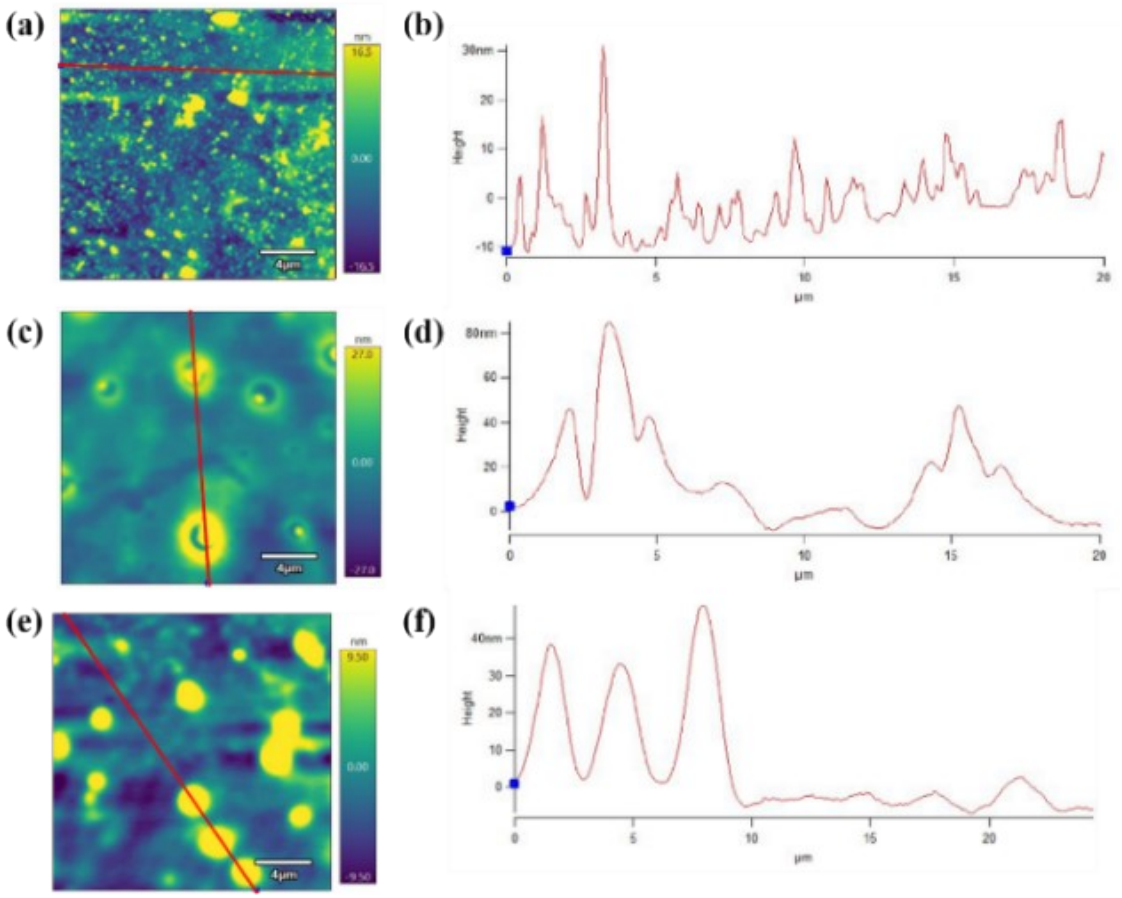

Figure S7 AFM image for complex **1**: height retrace: (a) Before reaction (c) Reacting 1 h image (e) After reaction; height profile charts: (b):Before reaction (d) Reacting 1 h image (f) After reaction.

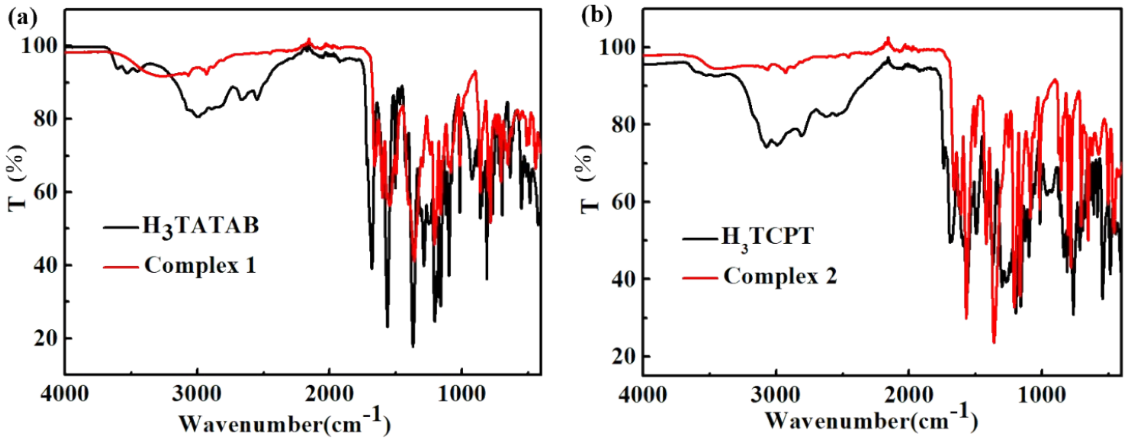

Figure S8 Infrared spectra: (a) Complex **1**; (b) Complex **2**

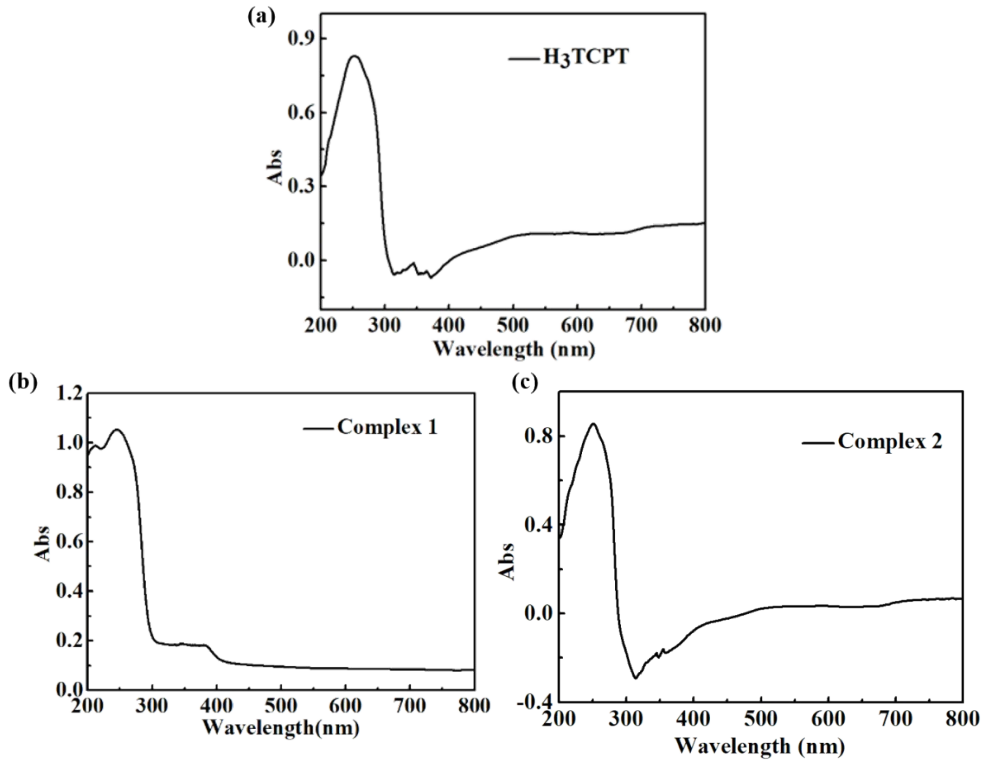

Figure S9 The UV-vis spectra: (a) H_3TCPT; (b) Complex **1**; (c) Complex **2**

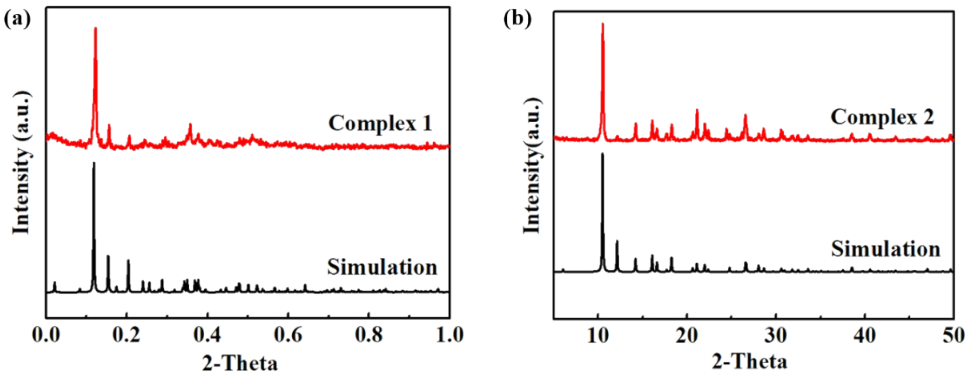

Figure S10 PXRD patterns (a) Complex **1**; (b) Complex **2**

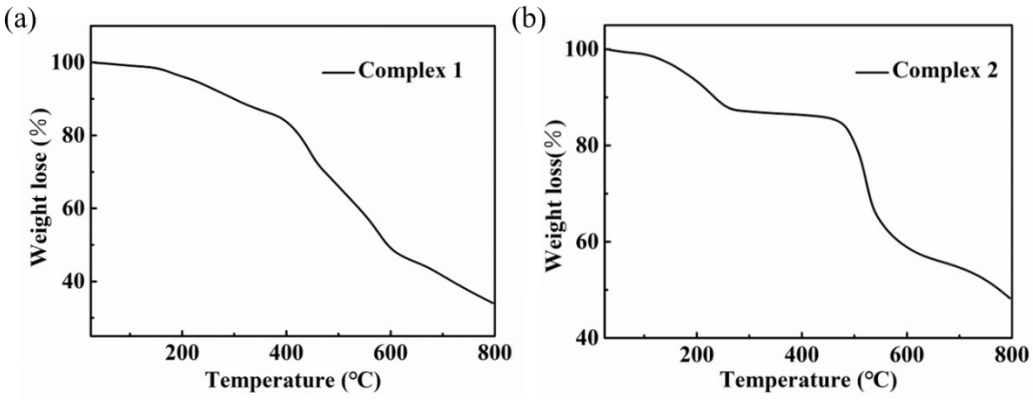

Figure S11 TG curves: (a) Complex **1**; (b) Complex **2**

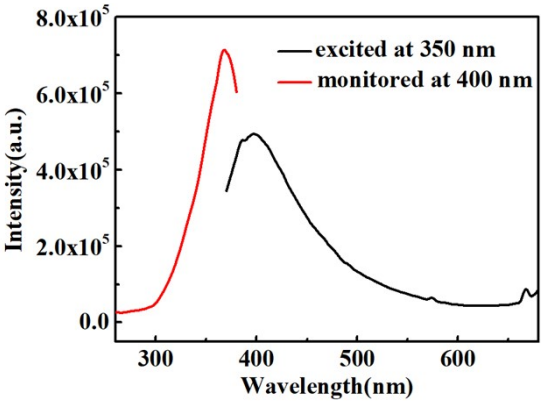

Figure S12 The excitation and emission spectra of H_3TCPT

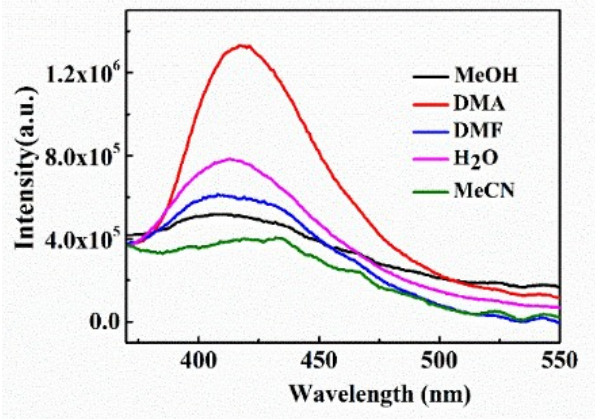

Figure S13 Fluorescence intensity of complex **1** in different solvents

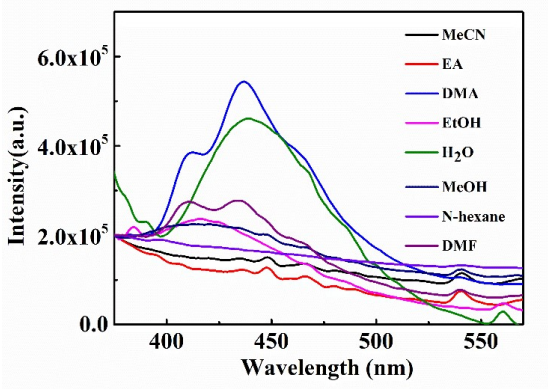

Figure S14 Fluorescence intensity of complex **2** in different solvents

Interference experiment of complex 1 detecting balsalazide sodium.

5 mg of complex **1** was dispersed in 5 mL of DMA and sonicated for 30 min at room temperature to prepare a suspension. 200 μL of 10^{-2} M solution of major components of serum was added to 2 mL suspension of complex **1**, respectively, and then 200 μL 10^{-2} M solution of balsalazide sodium was added. The fluorescence emission intensity at 425 nm was monitored. As shown in Figure S10, the fluorescence emission intensity of complex **1** was still quenched obviously in the presence of the main components of serum. Therefore, we conclude complex **1** selectively detect balsalazide sodium in the presence of the main components of serum.

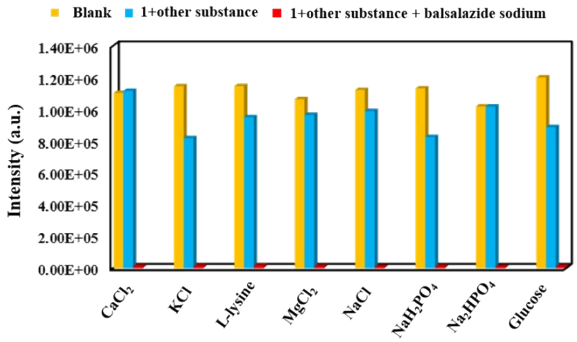

Figure S15 The effect of main components of serum on the detection of balsalazide disodium by complex **1**

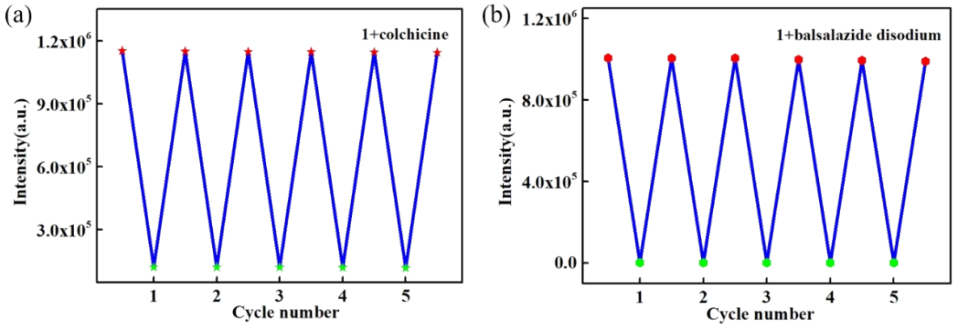

Figure S16 Recyclability test of **1** detecting small drug molecules: (a) Colchicine; (b) Balsalazide disoldium

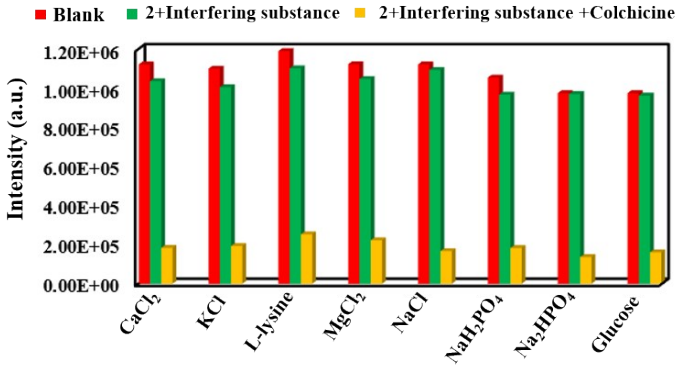

Figure S17 The effect of main components of serum on the detection of colchicine by complex **2**

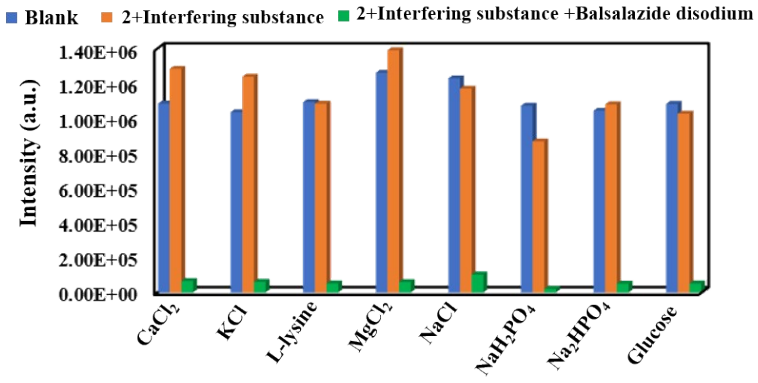

Figure S18 The effect of main components of serum on the detection of balsalazide disodium by

complex **2**

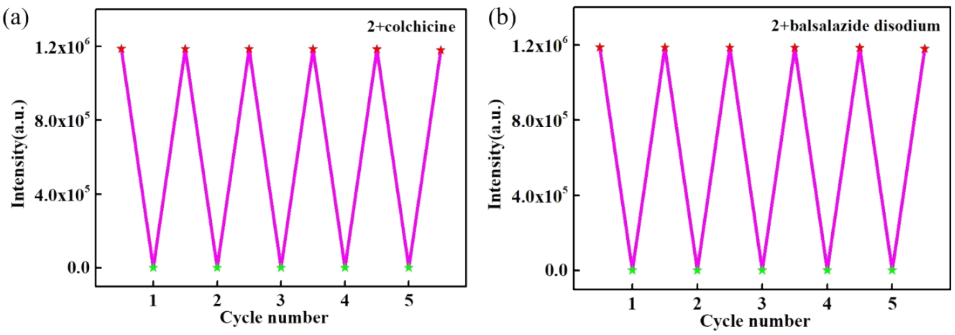

Figure S19 Recyclability test of **1** detecting small drug molecules: (a) Colchicine; (b) Balsalazide disoldium

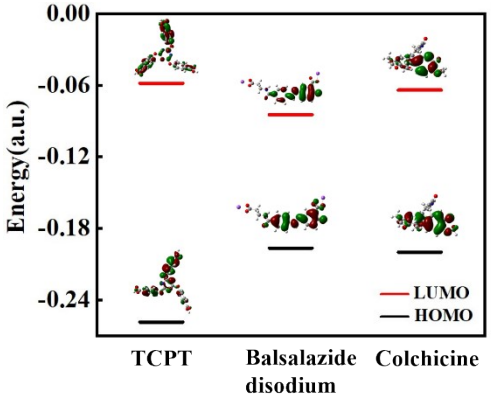

Figure S20 The molecular orbital energy levels of TCPT and small drug molecules

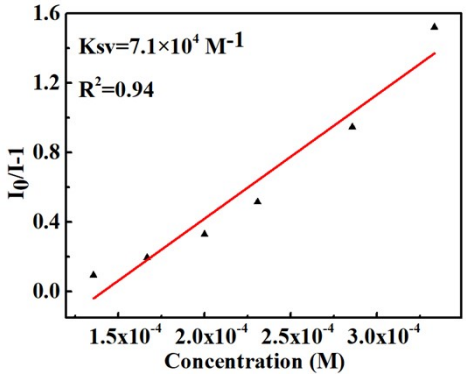

Figure S21 S-V linearity of fitting for complex **1** detecting of 10^{-2} M of MPD (200-1000 μL)

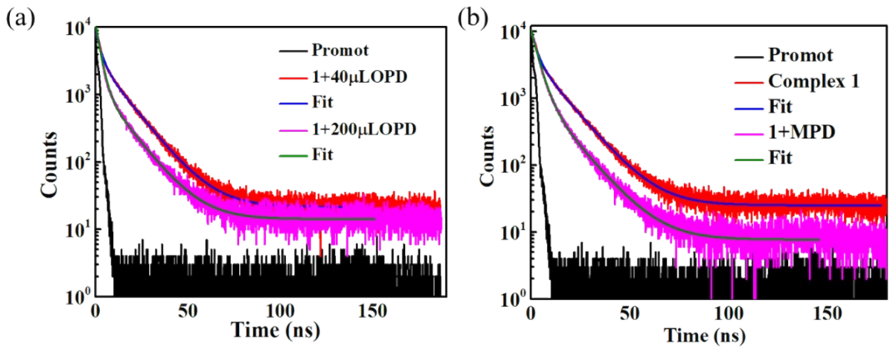

Figure S22 The fluorescence lifetime curve: (a) **1**+OPD; (b) **1**+MPD

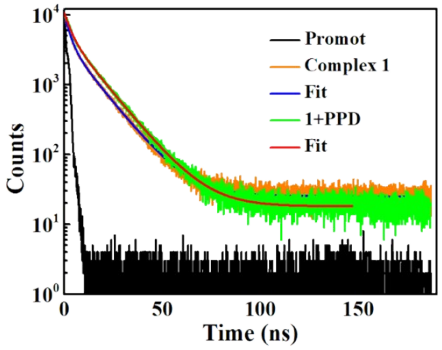

Figure S23 The fluorescence lifetime curve of complex **1**+PPD

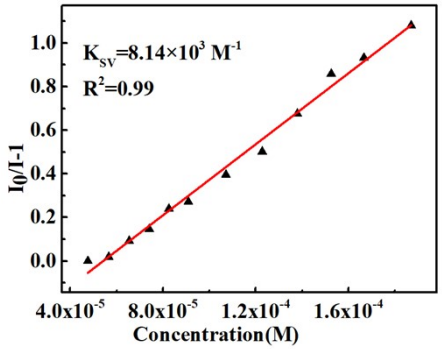

Figure S24 S-V linearity of complex **2** detectig 10^{-2} M OPD (100-1000 μL)

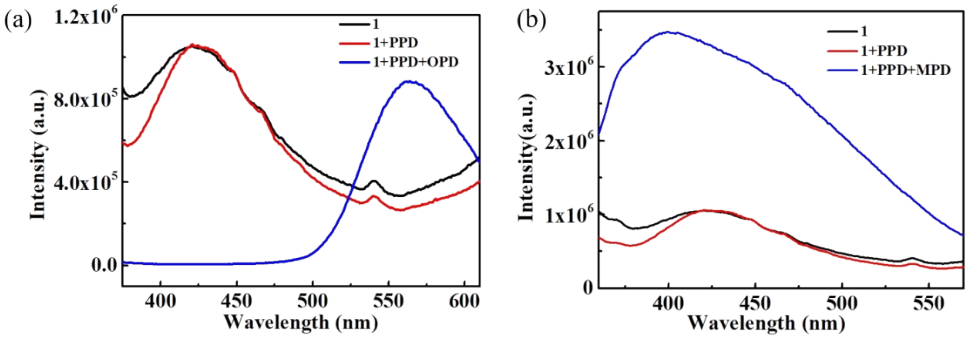

Figure S25 Interference experiment of PPD on the detection of OPD and MPD by complex **2**

References

[1] Aakeröy C B, Desper J, Urbina J F. Is conformational flexibility in a supramolecular reagent advantageous for high-yielding co-crystallization reactions? CrystEngComm, 2005; 7: 193-201.

[2] H. Wang, D. Liu, M. Wei, W. Qi, X. Li and Y. Niu, Environ Res, 2022, 208, 112652.

[3] Q. Lu, C. L. Copper and G. E. Collins, Anal Chim Acta, 2006, 572, 205-211.

[4] R. K. Kaja, K. V. Surendranath, P. Radhakrishnanand, J. Satish and P. V. V. Satyanarayana, Chromatographia, 2009, 69, 1007-1012.

[5] R. Huo, Y. Sun, Y. H. Xing, F. Y. Bai and L. X. Sun, J Mol Struct, 2021, 1228, 12973.

[6] K. Jiang, S. Sun, L. Zhang, Y. Lu, A. Wu, C. Cai and H. Lin, Angew Chem Int Ed Engl, 2015, 54, 5360-5363.